

# An Intervention-Based Framework for Shortcut Diagnosis in Spoofing Countermeasures

Santiago Rubio<sup>1</sup>, Pilar Bello<sup>2</sup>, Dayana Ribas<sup>1,2</sup>, Antonio Miguel<sup>1</sup>, Eduardo Lleida<sup>1</sup>, Alfonso Ortega<sup>1</sup>

<sup>1</sup>ViVoLab, Aragón Institute for Engineering Research (I3A), University of Zaragoza, Spain

<sup>2</sup>BTS, Business Telecommunications Services, Spain

s.rubio@unizar.es, pbellobardaji@gmail.com, dribas@bts.io,  
{amiguel, lleida, ortega}@unizar.es

## Abstract

While deepfake audio detection systems achieve high performance in controlled benchmarks, their reliability often diminishes in the wild. Prior work shows that dataset-specific artifacts contribute to this gap. Yet, systematic tools to identify which acoustic properties a model exploits as shortcuts remain limited. We propose an intervention-based diagnostic framework, grounded in a directed graphical model, that formally distinguishes confound-driven shortcut dependencies from legitimate domain shift. We operationalise this through controlled acoustic perturbations targeting non-speech structure, spectral content, and signal energy, complemented by corpus-level distributional analysis. Evaluating XLS-R-300M with RawGAT-ST across ASVspoof challenges datasets, we quantify model sensitivity to specific intervention types. Results reveal that non-speech interventions produce the largest performance shifts, confirming non-speech intervals as a dominant shortcut.

**Index Terms:** Audio Deepfake Detection, Data Augmentation, Shortcut Learning, Generalization

## 1. Introduction

Detecting synthetic speech has become a critical challenge, and deep learning models have seemingly risen to the occasion, achieving remarkably low error rates on standard benchmarks [1, 2]. However, this success is often an illusion. When these highly accurate models are tested in the wild, facing new datasets, different scenarios, or unseen attacks, their performance frequently collapses [3, 4, 5, 6]. This persistent generalisation gap undermines confidence across almost all architectures, from traditional classifiers [7, 8, 9] to the current state-of-the-art based on large self-supervised (SSL) front-ends [10, 11, 12] and advanced back-ends [13, 14, 15, 16].

This vulnerability is often driven by “shortcut learning” [17]. A shortcut occurs when a model relies on accidental cues in the dataset that happen to separate real from spoofed audio, rather than learning the actual artifacts of the generation process. If systems depend heavily on these shortcuts, their reported benchmark metrics may dangerously overestimate real-world robustness. Evidence strongly supports this concern: dataset artifacts in anti-spoofing benchmarks were first documented in ASVspoof 2017 [18, 19], and later editions revealed systematic differences in non-speech distributions between bonafide and spoofed audio [20]. The design of ASVspoof 5 explicitly acknowledges this problem by trimming non-speech intervals and normalising energy to mitigate these shortcuts [21], a concern echoed in independent analyses [22].

Beyond non-speech artifacts, external factors like codec compression and channel effects cause further degradation [4, 5]. While the community has responded with data augmentation, laundering-based simulation [23], guided masking [24],

and synthesis-based diversification [25], SSL front-ends still retain a consistent advantage under open conditions [26]. This suggests they naturally absorb part of the robustness burden that augmentation targets in classical systems.

Despite these efforts, the field lacks a formal way to characterise shortcut learning beyond simply documenting individual artifacts [17, 19, 20]. Existing work identifies shortcut candidates through empirical perturbation studies [27, 28] or proposes augmentation-based fixes, but stops short of grounding shortcut dependency in the data-generating process. One line of work demonstrates that shortcuts can be deliberately constructed or suppressed; another quantifies bias through black-box statistical frameworks, yet neither provides a formal criterion to determine *whether* a performance drop reflects spurious correlation exploitation or genuine distribution mismatch, the diagnostic question this paper directly addresses.

This paper addresses this diagnostic gap through three contributions. First, we formalise the data-generating process of spoofing corpora as a directed graphical model that distinguishes intrinsic synthesis artifacts ( $Z$ ) from idiosyncratic pipeline choices ( $C_d$ ) and exogenous channel effects ( $C_i$ ), and derive a definition of confounded shortcut dependency grounded in the conditional independence structure of the graph. Second, we operationalise this framework through a battery of controlled acoustic perturbations, targeting non-speech structure, spectral content, and signal energy, designed to selectively modify candidate shortcut features while preserving the intrinsic generative content, and measure sensitivity through the relative degradation in detection cost under each perturbation. Third, we apply the complete framework to a hybrid architecture pairing XLS-R-300M [12] with RawGAT-ST [13, 29] across ASVspoof 2019 LA [30], ASVspoof 2021 LA [4], and ASVspoof 5 [6], evaluating five training configurations that span frozen and fine-tuned SSL front-ends, with and without data augmentation, to isolate the effect of front-end adaptation on shortcut sensitivity.

## 2. Problem Formulation

### 2.1. Task Definition and Notation

Let  $\mathbf{x} \in \mathbb{R}^T$  denote a raw speech waveform of  $T$  samples and let  $S \in \{0, 1\}$  indicate the true nature of the utterance, where  $S=1$  denotes bonafide and  $S=0$  spoofed. A hybrid spoofing countermeasure learns a mapping  $f_\theta: \mathbb{R}^T \rightarrow [0, 1]$ , decomposed as  $f_\theta = h_\psi \circ g_\phi$ , where  $g_\phi$  is a self-supervised front-end that produces a sequence of frame-level representations  $\mathbf{R} = g_\phi(\mathbf{x})$ , and  $h_\psi$  is a downstream classifier that maps  $\mathbf{R}$  to a scalar score  $s = h_\psi(\mathbf{R}) \in \mathbb{R}$ , yielding a binary prediction  $\hat{S} = \mathbf{1}[s > \tau]$  for threshold  $\tau$ . We denote by  $\hat{Z}$  the internal utterance-level representations learned by the model; whether  $\phi$  is held frozen

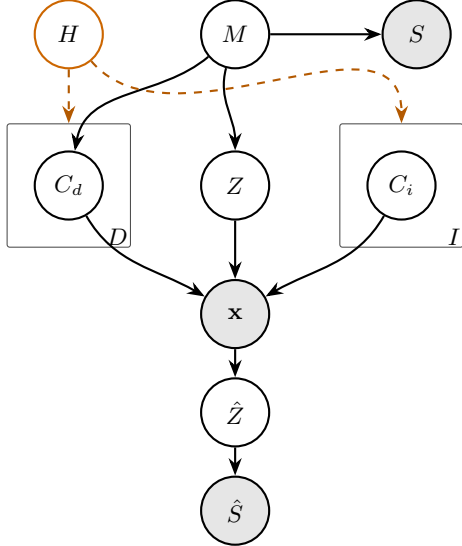


Figure 1: *Directed graphical model of the data-generating process and diagnostic framework* [31, 32]. *Shaded nodes: observed* ( $\mathbf{x}$ ,  $S$ ,  $\hat{S}$ ); *Solid nodes: latent* ( $M$ ,  $Z$ ,  $C_d$ ,  $C_i$ ,  $\hat{Z}$ ). *Plates  $D$  and  $I$  index the sets of idiosyncratic and exogenous factors*. *Orange dashed arrows denote controlled interventions  $H$*

or updated during training constitutes a variable of the analysis. The parameter set  $\theta = \{\phi, \psi\}$  is optimised over a training corpus  $\mathcal{D}_{\text{train}} = \{(\mathbf{x}_i, S_i)\}_{i=1}^n$ .

## 2.2. Structure of the Data Generation Process

We frame the data generation and annotation as a graphical model, represented by the directed acyclic graph in Fig. 1. The generative mechanism  $M$  sets the true nature  $S$  of the utterance: if  $M$  is a human vocal tract, then bonafide; if  $M$  is a TTS or VC pipeline, then spoof. The corpus-assigned label  $S_i \in \{0, 1\}$  is a protocol-dependent realisation that reflects the labelling decisions of a specific dataset rather than a direct measurement of the underlying generative process. The mechanism  $M$  leaves two structurally distinct traces in the observed waveform:

- **$Z$ : Intrinsic Artifacts.** Fundamental “fingerprint” inherent to the synthesis process regardless of the specific implementation (e.g., vocoder phase anomalies). These are the robust, generalizable features that models should ideally learn.
- **$C_d$ : Idiosyncratic Artifacts.** Extrinsic acoustic characteristics dependent on the specific generation pipeline (e.g., unnatural non-speech distributions or peak normalization). While generated by  $M$ , they are extrinsic algorithmic choices rather than fundamental properties of spoofed speech.

Additionally, the observed waveform  $\mathbf{x}$  can be modulated by class-independent exogenous factors  $C_i$  (e.g., codecs or tx channel) which are causally disconnected from  $M$ . Crucially, the protocol design of any specific training corpus  $\mathcal{D}_{\text{train}}$  inevitably introduces a *spurious correlation* between the idiosyncratic artifacts  $C_d$  and the label  $S$ . Because datasets contain a limited diversity of generative pipelines, certain post-processing artifacts become strongly correlated with the spoofed class.

## 2.3. Confounded Shortcut Dependencies

Cross-condition degradation stems from two distinct failure modes: **Domain shift** arises when the distribution of one or more exogenous variables differs between training and evalua-

tion. In its most common form, a change in  $P(C_i)$  alters the marginal  $P(\mathbf{x})$ . This naturally degrades the performance of almost any model, but it does not mean the model learned the wrong features.

**Shortcut learning**, on the other hand, occurs when the model re-encodes spurious statistical regularities of the training corpus [17]. We formalise this with respect to the DAG in Fig. 1. Let  $\hat{Z}$  denote the internal representation learned by the model. The ideal countermeasure satisfies the *causal sufficiency condition* [32]:

$$\hat{Z} \perp\!\!\!\perp (C_d, C_i) \mid Z \quad (1)$$

that is, the model’s representation depends on the observed waveform  $\mathbf{x}$  only through the intrinsic artifacts  $Z$ , discarding both idiosyncratic pipeline choices  $C_d$  and exogenous channel effects  $C_i$ .

We say that the model exhibits a *confounded shortcut dependency* on  $C_d$  if the following conditions hold jointly:

- Confound-driven association.** Under the training distribution,  $C_d$  is statistically associated with the label  $S$ :

$$C_d \not\perp\!\!\!\perp S \mid \mathcal{D}_{\text{train}} \quad (2)$$

Crucially, this is not a true cause-and-effect relationship. The artifact  $C_d$  does not define whether an audio is a deepfake. Instead, this accidental correlation appears only because  $\mathcal{D}_{\text{train}}$  contains a limited diversity of mechanisms  $M$ , creating a confound-driven statistical pathway from  $C_d$  to  $S$ .

- Representational leakage.** The learned representation violates the sufficiency condition (Eq. 1) by encoding  $C_d$ :

$$\hat{Z} \not\perp\!\!\!\perp C_d \mid Z \quad (3)$$

Rather than relying on the path  $Z \rightarrow \mathbf{x} \rightarrow \hat{Z} \rightarrow \hat{S}$ , the model exploits  $C_d \rightarrow \mathbf{x} \rightarrow \hat{Z} \rightarrow \hat{S}$  — a path that is predictive under  $\mathcal{D}_{\text{train}}$  but unstable under distribution shift, precisely because the association  $C_d$ – $S$  is conditional on the training protocol rather than on the generative structure. This shortcut inflates benchmark scores but fails in the wild where this correlation vanishes.

As a result, when  $P_{\text{eval}}(C_d \mid S) \neq P_{\text{train}}(C_d \mid S)$ , the confound-driven association ceases to be predictive and performance degrades. This fragility is the observable symptom, not the definition, of the underlying failure. Unlike domain shift, which degrades any model and is typically addressed via data augmentation, shortcut degradation is a selective failure. A model relying on  $C_d$  will misclassify novel attacks not because the acoustic environment has changed, but because its decision boundary was never grounded in the generative structure of the task [21]. Diagnosing these shortcut dependencies requires controlled interventions that alter an estimation of  $C_d$  while preserving  $Z$ .

## 2.4. Diagnostic Strategy: From Interventions to Shortcut Evidence

Our framework defines a confounded shortcut dependency using two conditions: spurious dataset correlation (Eq. 2) and representational leakage (Eq. 3). While the first condition can be verified through corpus-level statistical analysis, the second requires empirical proof that the learned representation  $\hat{Z}$  encodes  $C_d$ . This section describes how controlled acoustic perturbations provide such evidence.

The ideal test would directly modify the idiosyncratic artifact  $C_d$  while holding  $Z$  fixed and observing whether the model prediction changes. In practice,  $C_d$  is latent and cannot be ma-

nipulated in isolation. What we can manipulate is the observed waveform  $\mathbf{x}$ . A key property of the framework makes this tractable: the intrinsic artifacts  $Z$  are imprinted in the waveform at generation time by the synthesis mechanism  $M$ , and no post-hoc perturbation applied to  $\mathbf{x}$  can alter them. Adding non-speech fragments, injecting noise, or filtering frequency bands cannot reverse or modify the acoustic fingerprint left by a vocoder or a TTS acoustic model. Perturbations can only modify  $C_d$  (e.g., non-speech structure),  $C_i$  (e.g., channel characteristics), or *mask* the observability of  $Z$  (e.g., by destroying the spectral region where  $Z$  is most evident), but they cannot change  $Z$  itself.

This distinction yields a clear inferential logic. This leads to a clear diagnostic logic: if we perturb a candidate artifact  $C_d$  without masking  $Z$ , and the model’s performance drops, the degradation reflects the model’s reliance on that shortcut. Non-speech perturbations are the perfect tool for this. They operate on non-speech regions where intrinsic generative traces are typically minimal or easily overwritten by trivial post-processing. By modifying  $C_d$  without altering or masking  $Z$ , they provide an exceptionally clean diagnostic for shortcut dependence. In contrast, spectral and some energy perturbations are more ambiguous; a performance drop could mean either shortcut exploitation or the accidental masking of legitimate  $Z$  features.

Our diagnostic protocol proceeds as follows: for each candidate shortcut identified in the corpus (Section 3.2), we design a targeted perturbation or intervention, apply it to the evaluation data, and measure the resulting performance shift using relative DCF degradation ( $\delta_{m,p}$ ) (Section 3.4). Comparing these shifts across non-speech, spectral, and energy perturbations yields a *sensitivity profile* that precisely characterises which acoustic properties the model is actively exploiting.

### 3. Experimental Setup

#### 3.1. Architectural Configuration

The hybrid countermeasure follows the  $f_\theta = h_\psi \circ g_\phi$  formulation (Section 2.1, Fig. 2). The front-end  $g_\phi$  is XLS-R-300M [12], held frozen or fine-tuned. The classifier  $h_\psi$  follows the RawGAT-ST architecture [29], producing a time-independent embedding  $\hat{Z} \in \mathbb{R}^{160}$  mapped to two class logits.

**Training and Evaluation Corpora** The primary training corpus is ASVspooft 2019 LA<sup>1</sup> [30], comprising spoofed utterances from 6 TTS and voice conversion systems. The evaluation partition covers 13 additional unseen synthesis algorithms. A subset of models is additionally trained on a joint corpus combining ASVspooft 2019 LA and ASVspooft 5 training data [21]; the ASVspooft 5 training partition contains 8 TTS/VC systems, drawn from a broader set of 32 algorithms spanning the full corpus. All models are evaluated under three conditions of increasing domain distance: (i) **ASVspooft 2019 LA eval** [30], in-domain, unseen algorithms but matched recording conditions; (ii) **ASVspooft 2021 LA eval** [4], same TTS systems transmitted through telephone and VoIP codecs, introducing channel variability absent from training; and (iii) **ASVspooft 5 eval** [6], fully disjoint synthesis algorithms under crowdsourced and adversarially perturbed conditions.

**Training configuration.** All input waveforms are peak-normalised and adjusted to 64,600 samples ( $\approx 4$  s at 16 kHz).

<sup>1</sup>For brevity, all subsequent references to ASVspooft 2019 and 2021 refer exclusively to their Logical Access (LA) partitions.

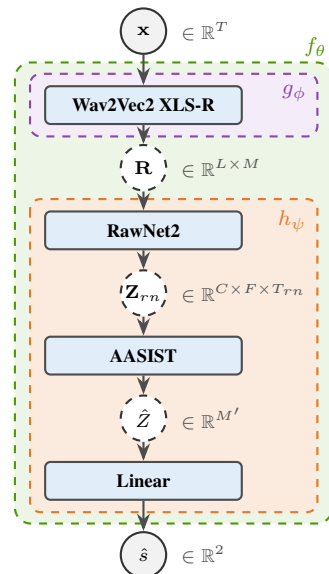


Figure 2: Detailed architecture of the proposed hybrid SSL-based spoofing detection model. Intermediate latent representations ( $\mathbf{R}$ ,  $\mathbf{Z}_{rn}$ ,  $\hat{Z}$ ) and dimensionalities are mapped along the data flow from input  $\mathbf{x}$  to the final score  $\hat{s}$ .

Models are trained for 30 epochs with batch size 24, Adam optimiser ( $\text{lr} = 10^{-6}$ , weight decay =  $10^{-4}$ ), and weighted cross-entropy with  $(w_{sp}, w_{bona}) = (0.1, 0.9)$ . Two augmentation regimes are compared. The first applies *RawBoost* (RB) [33], which introduces convolutive and impulsive additive noise on the raw waveform, with standard truncation/tiling for length normalisation. The second is a *custom pipeline* (DA), inspired by strategies from recent ASVspooft 5 submissions [26], that applies a stochastic chain of augmentations: non-speech trimming, RIR convolution [34], background noise addition at 8–20 dB SNR [35], RawBoost, codec simulation matching ASVspooft 2021 LA conditions [4], and time masking. Each stage is applied independently with a fixed probability, and 20% of samples pass through unchanged to preserve clean examples in the training distribution. Length normalisation in DA uses reflection padding with random circular shift instead of tiling.

#### 3.2. Corpus-Level Distributional Analysis

We extract eleven acoustic descriptors per utterance using Silero VAD [36]. To identify candidate shortcuts, Figure 3 plots the Jensen–Shannon divergence (JSD) [37] between bonafide and spoofed acoustic descriptors distributions for each descriptor. The  $x$ -axis shows separability in the training set, while the  $y$ -axis shows separability in the evaluation sets (high JSD denotes strong class separability). Additionally, the circle size encodes the distribution shift between train and evaluation sets: large circles indicate unstable properties across domains, whereas small circles denote stable descriptors.

In the ASVspooft 2019 panel, non-speech-related descriptors cluster in the upper-right, meaning they highly separate classes in both training and evaluation. However, they shift toward the lower-right in 2021, and nearly vanish in ASVspooft 5. This drop aligns perfectly with the ASVspooft 5 protocol, which explicitly trims non-speech regions and normalises energy in its evaluation data [21]. This pattern confirms non-speech intervals as a fragile shortcut: highly exploitable during training, but progressively useless as evaluation conditions change.

The arrows reveal a counterintuitive effect: adding

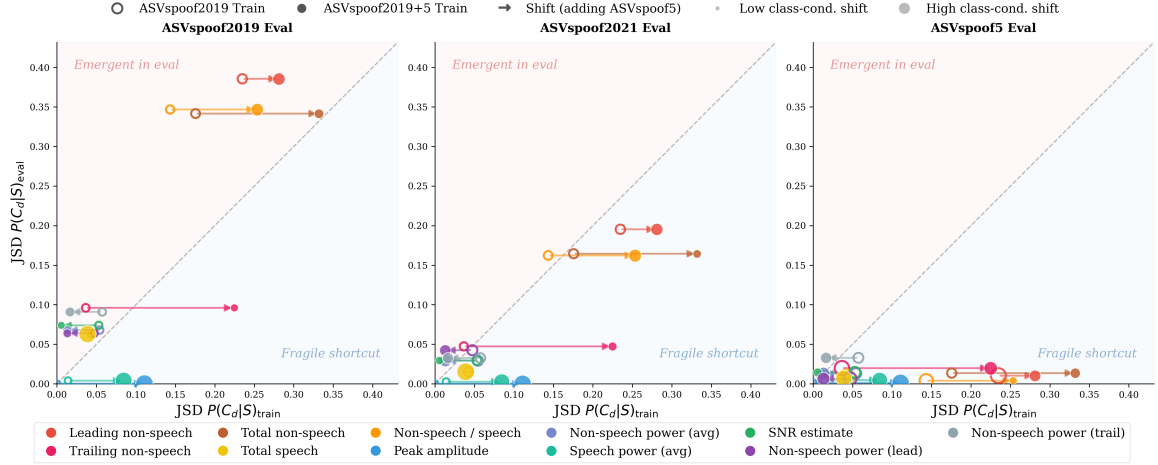


Figure 3: *Class separability across conditions: JSD between bonafide and spoofed distributions on the training partition (x-axis) vs. each evaluation set (y-axis). Hollow/filled markers: trained on ASV19 only / ASV19+ASV5; arrows: shift from adding AS5 data. Points in the lower-right are separable in training but not in evaluation (fragile shortcut).*

ASVspooF 5 training data increases the training-side bias for both non-speech and certain energy descriptors. This occurs because this training partition preserves the non-speech and energy asymmetries that its evaluation protocol suppresses [21]. Therefore, blindly expanding a corpus simply amplifies the confound if the new data carries the same biases. In contrast, signal quality descriptors remain stably near the origin, confirming they do not act as shortcuts regardless of the training corpus.

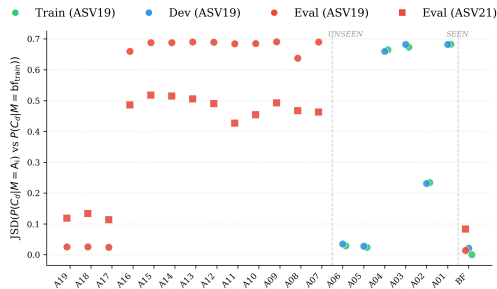


Figure 4: *Per-mechanism JSD for leading non-speech duration in ASV19 and ASV21, computed between the training bonafide distribution ASV19 and each attack or evaluation bonafide set.*

To understand this further, Figure 4 breaks down the JSD for leading non-speech regions, one of the strongest shortcuts, by specific attack algorithms across the 2019 and 2021 datasets. The high variance across different attacks confirms that the shortcut strength depends heavily on the specific synthesis mechanism ( $M$ ). Notably, the extreme separability observed for several attacks indicates they could be trivially classified by this property alone. Furthermore, the bonafide distribution in ASVspooF 2021 shifts drastically because its `only_speech` annotation [4] artificially strips leading non-speech regions. This reduction in class separability occurs independently of the spoofed class, proving that the shortcut is tied to the dataset’s protocol rather than the generative process itself.

### 3.3. Intervention Framework

Following the strategy in Section 2.4, we design controlled interventions targeting three acoustic categories: non-speech structure, spectral content, and signal energy. Table 1 summarises the set used in the reported experiments.

Non-speech manipulations constitute the largest group, reflecting the strong distributional asymmetry documented in Section 3.2. We inject 4.0 s of either zero-padding or AWGN (Additive White Gaussian Noise) at the beginning (lead) or end (trail) of the audio, substantially exceeding the non-speech durations observed in the training corpus. Spectral and energy interventions probe dependence on frequency content and amplitude/noise robustness, respectively. For peak normalisation, the target is drawn from a narrow distribution centred at the nominal value (0.65 or 0.45) to avoid introducing a perfectly deterministic artificial cue. Intervention-based diagnosis is conducted only on ASVspooF 2019 and 2021.

Table 1: *Controlled intervention set for shortcut probing, grouped by targeted acoustic property.*

Category	Perturbation	Parameters
Non-Speech	Zero padding	lead / trail, 4.0 s
	AWGN padding	lead / trail, 4.0 s
Spectral	Band-cut filter	0–2 / 2–5 / 5–8 kHz
	Downsample	8 kHz
Energy	Additive AWGN	20 / 10 / 5 dB SNR
	Peak normalisation	$\mu = 0.65 / \mu = 0.45$

### 3.4. Evaluation Metrics

Baseline performance is reported as Equal Error Rate (EER) across all conditions. For calibrated decision analysis we use the normalised detection cost function (DCF) [38] with the cost parameters and spoofing prior defined in the ASVspooF 2019 evaluation protocol [30], consistent across all three evaluation corpora. The global threshold  $\tau^*$  is obtained by minimising the DCF on the clean evaluation set and held fixed across all subsequent analyses. To quantify the impact of each perturbation we measure the relative degradation in DCF:

$$\delta_{m,p} = \frac{\text{DCF}_{m,p} - \text{DCF}_{m,\text{clean}}}{\text{DCF}_{m,\text{clean}}}, \quad (4)$$

where  $\text{DCF}_{m,p}$  and  $\text{DCF}_{m,\text{clean}}$  are the costs of model  $m$  on perturbed and clean data, respectively, both evaluated at  $\tau^*$ . Positive values indicate degradation. The relative formulation makes  $\delta_{m,p}$  comparable across perturbation types within the

	Model	Inter.	Base DCF	Spectral				Noise/Amp					Non-Speech			
				S1	S2	S3	S4	N1	N2	N3	N4	N5	T1	T2	T3	T4
ASVspooF 2019 eval	RB-19*	<i>Spoof</i> <i>Both</i>	0.109	-0.34 <b>+15.96</b>	+0.08 <b>+0.30</b>	-0.17 <b>+1.39</b>	-0.23 <b>+3.06</b>	+0.56 <b>+0.29</b>	+0.59 <b>+1.90</b>	+0.54 <b>+4.02</b>	+0.02 <b>+0.06</b>	+0.04 <b>+0.30</b>	+1.43 <b>+0.82</b>	+1.40 <b>+0.77</b>	+0.81 <b>+0.34</b>	+0.39 <b>-0.07</b>
	RB-19	<i>Spoof</i> <i>Both</i>	0.004	+14.25 <b>+32.99</b>	-0.14 <b>-0.14</b>	-0.26 <b>+0.07</b>	-0.28 <b>+0.25</b>	+0.80 <b>+0.67</b>	+2.85 <b>+2.65</b>	+5.20 <b>+5.07</b>	+0.13 <b>+0.13</b>	+0.22 <b>+0.22</b>	<b>+63.73</b>	+43.73 <b>+43.08</b>	<b>+65.95</b>	+44.25 <b>+43.60</b>
	DA-19	<i>Spoof</i> <i>Both</i>	0.203	-0.35 <b>+8.03</b>	+0.06 <b>+0.07</b>	+0.02 <b>+0.05</b>	+0.03 <b>+0.05</b>	+0.04 <b>+0.05</b>	+0.04 <b>+0.48</b>	-0.05 <b>+1.13</b>	+0.07 <b>+0.07</b>	+0.13 <b>+0.13</b>	+0.49 <b>-0.11</b>	+0.39 <b>-0.19</b>	+0.42 <b>-0.10</b>	+0.36 <b>-0.15</b>
	RB-24	<i>Spoof</i> <i>Both</i>	0.006	+6.96 <b>+71.43</b>	+1.26 <b>+4.66</b>	+0.14 <b>+0.58</b>	+0.05 <b>+2.84</b>	+1.14 <b>+1.01</b>	+1.26 <b>+9.28</b>	+1.43 <b>+49.66</b>	+0.55 <b>+0.38</b>	+1.28 <b>+1.11</b>	<b>+15.60</b>	+4.03 <b>+4.94</b>	<b>+18.83</b>	+2.84 <b>+13.95</b>
	DA-24	<i>Spoof</i> <i>Both</i>	0.261	-0.06 <b>+3.78</b>	+0.11 <b>+0.16</b>	+0.06 <b>+0.05</b>	+0.02 <b>+0.29</b>	-0.00 <b>+1.56</b>	-0.11 <b>+3.64</b>	-0.23 <b>+5.33</b>	+0.07 <b>-0.20</b>	+0.12 <b>-0.26</b>	-0.22 <b>+0.98</b>	-0.22 <b>+1.00</b>	-0.27 <b>+2.47</b>	-0.23 <b>+2.20</b>
ASVspooF 2021 eval	RB-19*	<i>Spoof</i> <i>Both</i>	0.736	-0.03 <b>+1.54</b>	+0.01 <b>-0.00</b>	-0.01 <b>+0.06</b>	-0.02 <b>+0.21</b>	+0.07 <b>-0.32</b>	+0.09 <b>-0.08</b>	+0.09 <b>+0.21</b>	-0.00 <b>+0.03</b>	-0.00 <b>+0.09</b>	+0.16 <b>-0.52</b>	+0.17 <b>-0.49</b>	+0.09 <b>-0.42</b>	+0.04 <b>-0.29</b>
	RB-19	<i>Spoof</i> <i>Both</i>	0.302	+0.17 <b>+2.79</b>	-0.00 <b>+0.31</b>	-0.00 <b>+0.02</b>	-0.00 <b>+0.15</b>	+0.01 <b>-0.14</b>	+0.02 <b>-0.12</b>	+0.05 <b>-0.02</b>	+0.00 <b>+0.07</b>	+0.00 <b>+0.16</b>	<b>+0.57</b>	+0.36 <b>-0.30</b>	<b>+0.67</b>	+0.40 <b>-0.30</b>
	DA-19	<i>Spoof</i> <i>Both</i>	0.442	-0.11 <b>+3.23</b>	+0.01 <b>+0.01</b>	+0.00 <b>-0.02</b>	+0.00 <b>+0.02</b>	+0.01 <b>+0.05</b>	+0.00 <b>+0.33</b>	-0.02 <b>+0.66</b>	+0.02 <b>-0.12</b>	+0.04 <b>-0.19</b>	+0.29 <b>-0.43</b>	+0.23 <b>-0.41</b>	+0.25 <b>-0.37</b>	+0.21 <b>-0.36</b>
	RB-24	<i>Spoof</i> <i>Both</i>	0.277	+0.15 <b>+3.12</b>	+0.04 <b>+0.18</b>	+0.00 <b>-0.02</b>	-0.00 <b>+0.14</b>	+0.03 <b>+0.02</b>	+0.03 <b>+0.37</b>	+0.04 <b>+1.37</b>	+0.02 <b>-0.14</b>	+0.05 <b>-0.20</b>	<b>+0.33</b>	+0.08 <b>-0.14</b>	<b>+0.37</b>	+0.05 <b>+0.39</b>
	DA-24	<i>Spoof</i> <i>Both</i>	0.481	-0.12 <b>+2.46</b>	+0.03 <b>+0.25</b>	+0.02 <b>-0.03</b>	+0.00 <b>+0.09</b>	-0.02 <b>+0.86</b>	-0.09 <b>+1.84</b>	-0.15 <b>+2.53</b>	+0.03 <b>-0.10</b>	+0.05 <b>-0.17</b>	-0.15 <b>+0.81</b>	-0.15 <b>+0.84</b>	-0.17 <b>+1.43</b>	-0.16 <b>+1.30</b>

Table 2: Relative degradation  $\delta_{m,p}$  (Eq. 4) under controlled interventions. Columns report individual perturbations grouped by category: Spectral (S1: band-cut 0–2 kHz, S2: 2–5 kHz, S3: 5–8 kHz, S4: downsample 8 kHz), Noise/Amp (N1: AWGN 20 dB, N2: 10 dB, N3: 5 dB, N4: peak norm  $\mu=0.65$ , N5:  $\mu=0.45$ ), and Non-Speech (T1: zeros leading, T2: zeros trailing, T3: AWGN leading, T4: AWGN trailing; all 4.0 s). Two intervention targets are compared: *Spoof*, only spoofed utterances perturbed; *Both*, both classes perturbed. Base DCF is the clean-condition cost at the globally optimised threshold  $\tau^*$ . \* denotes frozen SSL front-end.

same model, where the denominator is constant and the ranking is unaffected by baseline performance. When comparing across models, we additionally report absolute DCF values to ensure that large relative values are not artifacts of near-zero denominators. We apply this same measure to isolate codec-induced degradation in ASVspooF 2021.

## 4. Results and Analysis

This section presents the empirical application of the diagnostic framework developed in Section 2. We first establish the generalisation gap to frame our diagnostic question. Next, we test for shortcut dependency through perturbation-based interventions and representational analysis. Finally, we analyse codec and channel-driven degradation, providing contrastive evidence to distinguish true domain shift from shortcut exploitation.

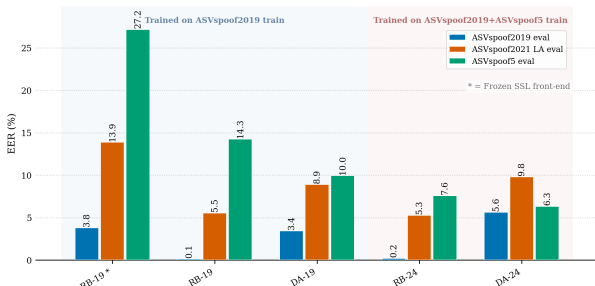


Figure 5: EER (%) across evaluation sets for all models.

### 4.1. Baseline Performance

Figure 5 reports EER across all evaluation conditions for four model configurations, which vary by augmentation strategy (RawBoost [RB] vs. custom data augmentation [DA]) and training corpus (ASVspooF 2019 alone [-19] vs. combined with ASVspooF 5 [-24]). While all models degrade progressively

from ASVspooF 2019 to ASVspooF 5, the magnitudes vary substantially. RB models achieve the lowest in-domain EER but suffer the steepest cross-corpus degradation, whereas DA models trade in-domain accuracy for better cross-corpus robustness. Expanding the training corpus yields expected evaluation gains for both approaches (RB-24, DA-24). Ultimately, however, the choice of augmentation strategy (DA vs. RB) dictates generalisation far more than simply adding data. This implies that severe cross-dataset degradation stems primarily from exploiting dataset-specific shortcuts rather than pure acoustic mismatch.

### 4.2. Intervention-Based Sensitivity Analysis

The generalisation gap in Section 2.3 stems from either acoustic domain mismatch ( $C_i$ ) or corpus-specific artefacts ( $C_d$ ). Since Section 3.2 identified non-speech as the primary condition (i) shortcut, Table 2 tests condition (ii) via sensitivity profiling.

**Low-frequency masking.** The 0–2 kHz band-cut (S1) yields a massive relative degradation ( $\delta$ ) under the *Both* target across all models, including DA. Rather than exposing a dataset shortcut ( $C_d$ ), this universal drop indicates the masking of legitimate generative traces ( $Z$ ). Removing this critical low-frequency content strips away intrinsic speech cues, artificially collapsing the boundary between bonafide and spoofed utterances in the representation space. In contrast, other spectral interventions exhibit consistent, moderate behaviour.

**Noise sensitivity in joint-corpus models.** Models trained on the joint ASV19+ASV5 corpus (RB-24, DA-24) exhibit substantially larger degradation under additive noise interventions, most markedly under the *Both* target, a pattern consistent across both ASVspooF 2019 and 2021 eval conditions. This is consistent with the distributional analysis of Section 3.2: adding ASV5 training data increases the class separability of speech and non-speech power descriptors (Fig. 3, rightward arrows), suggesting that joint-corpus models develop sensitivity to energy conditions that ASV19-only models do not exploit.

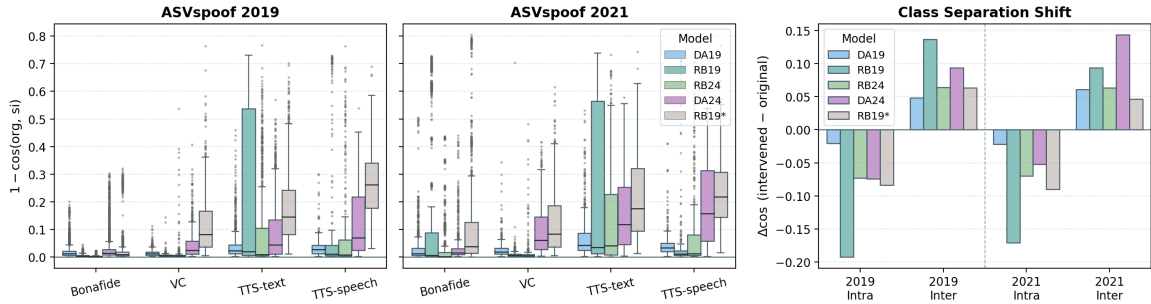


Figure 6: *Embedding analysis under non-speech intervention (2,000 balanced utterances). Left/centre: original intra-class cosine distance by input modality synthesis category. Right: intra- and inter-class  $\Delta$  cosine similarity (intervention – original). A negative inter-class  $\Delta$  indicates opposing classes move closer together.*

**Non-Speech Interventions.** The clearest pattern in Table 2 is the stark divergence between RB and DA models. RB-19 suffers an extreme degradation ( $\delta > 60$ ) under leading non-speech addition. Because this modification is strictly confined to non-speech regions where genuine generative traces ( $Z$ ) are absent, this performance drop unambiguously reflects reliance on the non-speech shortcut. Conversely, DA models, which are trained with non-speech trimming, show near-zero or negative  $\delta$ , confirming they are fully decoupled from  $C_d$ . Crucially, even though RB-24 is trained on a larger corpus (without non-speech augmentation), it still yields  $\delta = +18.83$ . This proves that simply scaling the dataset does not resolve the shortcut if the added data preserves the same confound.

**Cross-dataset attenuation.** On ASVspoof 2021 LA, non-speech  $\delta_{m,p}$  drops sharply, RB-19 falls from  $\delta_{m,p} > 60$  to  $\delta_{m,p} = +0.67$  for the same intervention, consistent with the protocol-level neutralisation of the  $C_d$ - $S$  association documented in Section 3.2. Notably, under *Both*,  $\delta_{m,p}$  turns negative for most models: the *only\_speech* annotation applied by the ASVspoof 2021 authors [4], itself an intervention on the bonafide non-speech distribution, partially disrupts the training-distribution profile; uniform non-speech addition partially restores it, recovering borderline decisions.

**Representational Leakage** To verify whether this non-speech bias is hardcoded into the learned representation ( $\hat{Z}$ ), Figure 6 visualises the embedding geometry under intervention. The left and centre panels measure the raw displacement caused by leading non-speech fragments, showing that RB embeddings shift drastically from their original state. Notably, for RB-19, the magnitude of this displacement varies substantially across different attack mechanisms, highlighting how deeply the shortcut’s influence is entangled with specific synthesis algorithms. More importantly, the right panel illustrates how this shift corrupts class separation: for RB models in ASVspoof 2019, adding non-speech fragments simultaneously scatters embeddings of the same class (negative intra-class  $\Delta$ ) and pulls opposing classes closer together (positive inter-class  $\Delta$ ). This blurring of the decision boundary is the definitive proof for condition (ii): rather than isolating intrinsic generative features ( $Z$ ), the model actively relies on non-speech structure ( $C_d$ ) to classify. Had the model successfully ignored the shortcut, its embeddings would remain invariant.

**Codec and Channel Consistency.** Codec and transmission conditions in ASVspoof 2021 LA provide the contrastive test for  $C_i$ -driven domain shift. Unlike non-speech interventions, where RB and DA models diverge by two orders of magnitude, codec-induced degradation is moderate and consistent across configurations: GSM produces the highest values (up to

$\delta_{m,p} = +4.06$ ) yet RB-19 and DA-19 show comparable sensitivity (+0.81 vs. +0.68), and G722 is effectively transparent for all models. Transmission path effects follow the same pattern, with *mad\_tx* producing the highest degradation across all configurations without interaction with augmentation strategy. This uniformity is the diagnostic signature of  $C_i$ -driven shift: the exogenous factor degrades all models equally since it does not operate through the  $C_d$ - $S$  confound, validating the framework’s core distinction between domain shift and shortcut exploitation. On ASVspoof 5, degradation magnitudes are larger due to more aggressive channel conditions, yet the relative ordering between models remains stable across conditions, confirming the same  $C_i$ -driven pattern at greater domain distance.

## 5. Conclusion

In this paper, we have proposed an intervention-based diagnostic framework that formally distinguishes shortcut learning from legitimate domain shift in spoofing countermeasures. By grounding our analysis in a directed acyclic graph, we derived the necessary conditions to identify when a model abandons the true generative footprint ( $Z$ ) to exploit spurious correlations stemming from idiosyncratic pipeline artifacts ( $C_d$ ), a phenomenon that artificially inflates performance in controlled benchmarks but causes severe degradation in the wild.

Our empirical results, obtained through controlled acoustic perturbations, confirm that non-speech structure acts as the dominant shortcut in standard corpora. Simple interventions in non-speech regions produce extreme degradation ( $\delta_{m,p} > 60$ ) in models trained with standard augmentations (RB), whereas strategies directly targeting the shortcut (such as non-speech trimming in DA) successfully decouple the decision boundary from the  $C_d$  artifact. However, this mitigation comes at a cost, as it considerably degrades overall performance compared to the original RawBoost baseline. Crucially, we demonstrate that simply scaling the corpus size by combining datasets is insufficient to resolve shortcut dependency if the training protocol does not explicitly mitigate these spurious correlations.

Looking forward, the separation between generative and idiosyncratic artifacts formalized in this study opens a promising research direction. This framework can guide the introduction of source tracing techniques and the application of minimal information criteria during training. Forcing networks to strictly retain the minimal information necessary to isolate the synthesis footprint, while penalizing the encoding of peripheral approximation to confounding variables, will be a fundamental step toward generating latent representations that are inherently robust and generalizable to unseen attacks.

## 6. Acknowledgements

This work has received funding from MCIN/AEI/10.13039/501100011033 under Grant PID2024-155948OB-C53.

## 7. References

- [1] Y. Zhu, C. Goel, S. Koppiseti, T. Tran, A. Kumar, and G. Bharaj, "Learn from real: reality defender's submission to ASVspoof5 Challenge," in *The Automatic Speaker Verification Spoofing Countermeasures Workshop (ASVspoof 2024)*, 2024, pp. 116–123.
- [2] Y. Xie, X. Wang, Z. Wang, R. Fu, W. Zhengqi, H. Cheng, and L. Ye, "Temporal variability and multi-viewed self-supervised representations to tackle the ASVspoof5 Deepfake Challenge," in *The Automatic Speaker Verification Spoofing Countermeasures Workshop (ASVspoof 2024)*, 2024, pp. 101–108.
- [3] N. Müller, P. Czempin, F. Diekmann, A. Froghyar, and K. Böttinger, "Does Audio Deepfake Detection Generalize?" in *Interspeech 2022*, 2022, pp. 2783–2787.
- [4] X. Liu, X. Wang, M. Sahidullah, J. Patino, H. Delgado, T. Kinnunen, M. Todisco, J. Yamagishi, N. Evans, A. Nautsch, and K. A. Lee, "Asvspoof 2021: Towards spoofed and deepfake speech detection in the wild," *IEEE/ACM Transactions on Audio, Speech, and Language Processing*, vol. 31, pp. 2507–2522, 2023.
- [5] P. Falez and T. Marteau, "Whisper speech deepfake detection systems for the ASVspoof5 Challenge," in *The Automatic Speaker Verification Spoofing Countermeasures Workshop (ASVspoof 2024)*, 2024, pp. 32–35.
- [6] X. Wang, H. Delgado, H. Tak, J. weon Jung, H. jin Shim, M. Todisco, I. Kukanov, X. Liu, M. Sahidullah, T. Kinnunen, N. Evans, K. A. Lee, and J. Yamagishi, "Asvspoof 5: Crowdsourced speech data, deepfakes, and adversarial attacks at scale," 2024. [Online]. Available: <https://arxiv.org/abs/2408.08739>
- [7] J. Rohdin, L. Zhang, P. Oldřich, V. Staněk, D. Mihola, J. Peng, T. Stafylakis, D. Beveraki, A. Silnova, J. Brukner, and L. Burget, "BUT systems and analyses for the ASVspoof 5 Challenge," in *The Automatic Speaker Verification Spoofing Countermeasures Workshop (ASVspoof 2024)*, 2024, pp. 24–31.
- [8] D. Combei, A. Stan, D. Oneata, and H. Cucu, "WavLM model ensemble for audio deepfake detection," in *The Automatic Speaker Verification Spoofing Countermeasures Workshop (ASVspoof 2024)*, 2024, pp. 170–175.
- [9] A. Kulkarni, H. M. Tran, A. Kulkarni, S. Dowerah, D. Lolive, and M. M. Doss, "Exploring generalization to unseen audio data for spoofing: insights from SSL models," in *The Automatic Speaker Verification Spoofing Countermeasures Workshop (ASVspoof 2024)*, 2024, pp. 86–93.
- [10] A. Baeviski, Y. Zhou, A. Mohamed, and M. Auli, "wav2vec 2.0: A framework for self-supervised learning of speech representations," in *Advances in Neural Information Processing Systems*, H. Larochelle, M. Ranzato, R. Hadsell, M. Balcan, and H. Lin, Eds., vol. 33. Curran Associates, Inc., 2020, pp. 12 449–12 460. [Online]. Available: [https://proceedings.neurips.cc/paper\\_files/paper/2020/file/92d1e1eb1cd6f9fba3227870bb6d7f07-Paper.pdf](https://proceedings.neurips.cc/paper_files/paper/2020/file/92d1e1eb1cd6f9fba3227870bb6d7f07-Paper.pdf)
- [11] S. Chen, C. Wang, Z. Chen, Y. Wu, S. Liu, Z. Chen, J. Li, N. Kanda, T. Yoshioka, X. Xiao, J. Wu, L. Zhou, S. Ren, Y. Qian, Y. Qian, J. Wu, M. Zeng, X. Yu, and F. Wei, "Wavlm: Large-scale self-supervised pre-training for full stack speech processing," *IEEE Journal of Selected Topics in Signal Processing*, vol. 16, no. 6, p. 1505–1518, Oct. 2022. [Online]. Available: <http://dx.doi.org/10.1109/JSTSP.2022.3188113>
- [12] A. Babu, C. Wang, A. Tjandra, K. Lakhotia, Q. Xu, N. Goyal, K. Singh, P. von Platen, Y. Saraf, J. Pino, A. Baeviski, A. Conneau, and M. Auli, "Xls-r: Self-supervised cross-lingual speech representation learning at scale," 2021. [Online]. Available: <https://arxiv.org/abs/2111.09296>
- [13] J.-w. Jung, H.-S. Heo, H. Tak, H.-j. Shim, J. S. Chung, B.-J. Lee, H.-J. Yu, and N. Evans, "Aasist: Audio anti-spoofing using integrated spectro-temporal graph attention networks," in *arXiv preprint arXiv:2110.01200*, 2021.
- [14] K. Borodin, V. Kudryavtsev, D. Korzh, A. Efimenko, G. Mkrtchian, M. Gorodnichev, and O. Y. Rogov, "AASIST3: KAN-enhanced AASIST speech deepfake detection using SSL features and additional regularization for the ASVspoof 2024 Challenge," in *The Automatic Speaker Verification Spoofing Countermeasures Workshop (ASVspoof 2024)*, 2024, pp. 48–55.
- [15] A.-T. Dao, M. Rouvier, and D. Matrouf, "ASVspoof 5 Challenge: advanced ResNet architectures for robust voice spoofing detection," in *The Automatic Speaker Verification Spoofing Countermeasures Workshop (ASVspoof 2024)*, 2024, pp. 163–169.
- [16] P.-C. Chan, W.-Y. Chen, and J.-C. Wang, "Enhancing spoofing detection in ASVspoof 5 Workshop 2024: fusion of WavLM-ResNet18-SA for optimal performance against speech deepfakes," in *The Automatic Speaker Verification Spoofing Countermeasures Workshop (ASVspoof 2024)*, 2024, pp. 158–162.
- [17] R. Geirhos, J.-H. Jacobsen, C. Michaelis, R. Zemel, W. Brendel, M. Bethge, and F. A. Wichmann, "Shortcut learning in deep neural networks," *Nature Machine Intelligence*, vol. 2, no. 11, p. 665–673, Nov. 2020. [Online]. Available: <http://dx.doi.org/10.1038/s42256-020-00257-z>
- [18] H. Delgado, M. Todisco, M. Sahidullah, N. Evans, T. Kinnunen, K. A. Lee, and J. Yamagishi, "ASVspoof 2017 Version 2.0: metadata analysis and baseline enhancements," in *The Speaker and Language Recognition Workshop (Odyssey 2018)*, 2018, pp. 296–303.
- [19] B. Chettri, E. Benetos, and B. L. T. Sturm, "Dataset artefacts in anti-spoofing systems: A case study on the asvspoof 2017 benchmark," *IEEE/ACM Transactions on Audio, Speech, and Language Processing*, vol. 28, pp. 3018–3028, 2020.
- [20] N. Müller, F. Diekmann, P. Czempin, R. Canals, K. Böttinger, and J. Williams, "Speech is Silver, Silence is Golden: What do ASVspoof-trained Models Really Learn?" in *2021 Edition of the Automatic Speaker Verification and Spoofing Countermeasures Challenge*, 2021, pp. 55–60.
- [21] X. Wang, H. Delgado, H. Tak, J. weon Jung, H. jin Shim, M. Todisco, I. Kukanov, X. Liu, M. Sahidullah, T. Kinnunen, N. Evans, K. A. Lee, J. Yamagishi, M. Jeong, G. Zhu, Y. Zang, Y. Zhang, S. Maiti, F. Lux, N. Müller, W. Zhang, C. Sun, S. Hou, S. Lyu, S. Le Maguer, C. Gong, H. Guo, L. Chen, and V. Singh, "Asvspoof 5: Design, collection and validation of resources for spoofing, deepfake, and adversarial attack detection using crowdsourced speech," *Computer Speech & Language*, vol. 95, p. 101825, 2026. [Online]. Available: <https://www.sciencedirect.com/science/article/pii/S0885230825000506>
- [22] J. M. Martín-Doñas, A. Álvarez, E. Rosello, A. M. Gomez, and A. M. Peinado, "Exploring Self-supervised Embeddings and Synthetic Data Augmentation for Robust Audio Deepfake Detection," in *Interspeech 2024*, 2024, pp. 2085–2089.
- [23] A. Aliyev and A. Kondratev, "Intema system description for the ASVspoof5 Challenge: power weighted score fusion," in *The Automatic Speaker Verification Spoofing Countermeasures Workshop (ASVspoof 2024)*, 2024, pp. 152–157.
- [24] D.-T. Truong, Y. Wang, K. A. Lee, M. Li, H. Nishizaki, and E. S. Chng, "A study of guided masking data augmentation for deepfake speech detection," in *The Automatic Speaker Verification Spoofing Countermeasures Workshop (ASVspoof 2024)*, 2024, pp. 176–180.
- [25] Y. Chen, H. Wu, N. Jiang, X. Xia, Q. Gu, Y. Hao, P. Cai, Y. Guan, J. Wang, W.-L. Xie, L. Fang, S. Fang, Y. Song, W. Guo, L. Liu, and M. Xu, "USTC-KXDIGIT system description for ASVspoof5 Challenge," in *The Automatic Speaker Verification Spoofing Countermeasures Workshop (ASVspoof 2024)*, 2024, pp. 109–115.

- [26] K. Schäfer, J.-E. Choi, and M. Neu, “Robust audio deepfake detection: exploring front-/back-end combinations and data augmentation strategies for the ASVspoof5 Challenge,” in *The Automatic Speaker Verification Spoofing Countermeasures Workshop (ASVspoof 2024)*, 2024, pp. 56–63.
- [27] H. jin Shim, R. Gonzalez Hautamäki, M. Sahidullah, and T. Kinnunen, “How to Construct Perfect and Worse-than-Coin-Flip Spoofing Countermeasures: A Word of Warning on Shortcut Learning,” in *Interspeech 2023*, 2023, pp. 785–789.
- [28] M. Sahidullah, H.-j. Shim, R. G. Hautamäki, and T. H. Kinnunen, “Shortcut learning in binary classifier black boxes: Applications to voice anti-spoofing and biometrics,” *IEEE Journal of Selected Topics in Signal Processing*, 2025.
- [29] H. Tak, J. weon Jung, J. Patino, M. Kamble, M. Todisco, and N. Evans, “End-to-end spectro-temporal graph attention networks for speaker verification anti-spoofing and speech deepfake detection,” in *Proc. 2021 Edition of the Automatic Speaker Verification and Spoofing Countermeasures Challenge*, 2021, pp. 1–8.
- [30] M. Todisco, X. Wang, V. Vestman, M. Sahidullah, H. Delgado, A. Nautsch, J. Yamagishi, N. Evans, T. H. Kinnunen, and K. A. Lee, “Asvspoof 2019: Future horizons in spoofed and fake audio detection,” in *Interspeech 2019*, 2019, pp. 1008–1012.
- [31] C. Bishop, *Pattern recognition and machine learning*. Springer New York, 2006, vol. 4. [Online]. Available: [http://scholar.google.com/scholar.bib?q=info:jYxggZ6Ag1YJ:scholar.google.com/&output=citation&hl=en&as\\_sdt=0,5&as\\_vis=1&ct=citation&cd=0](http://scholar.google.com/scholar.bib?q=info:jYxggZ6Ag1YJ:scholar.google.com/&output=citation&hl=en&as_sdt=0,5&as_vis=1&ct=citation&cd=0)
- [32] J. Pearl, *Causality: Models, Reasoning and Inference*, 2nd ed. USA: Cambridge University Press, 2009.
- [33] H. Tak, M. Kamble, J. Patino, M. Todisco, and N. Evans, “Rawboost: A raw data boosting and augmentation method applied to automatic speaker verification anti-spoofing,” in *IEEE International Conference on Acoustics, Speech and Signal Processing (ICASSP)*, 2022.
- [34] T. Ko, V. Peddinti, D. Povey, M. L. Seltzer, and S. Khudanpur, “A study on data augmentation of reverberant speech for robust speech recognition,” in *Proc. ICASSP*, 2017, pp. 5220–5224.
- [35] D. Ribas, A. Miguel, A. Ortega, and E. Lleida, “Wiener filter and deep neural networks: A well-balanced pair for speech enhancement,” *Applied Sciences*, vol. 12, no. 18, 2022. [Online]. Available: <https://www.mdpi.com/2076-3417/12/18/9000>
- [36] S. Team, “Silero vad: pre-trained enterprise-grade voice activity detector (vad), number detector and language classifier,” <https://github.com/snakers4/silero-vad>, 2024.
- [37] J. Lin, “Divergence measures based on the shannon entropy,” *IEEE Transactions on Information Theory*, vol. 37, no. 1, pp. 145–151, 1991.
- [38] T. Kinnunen, H. Delgado, N. Evans, K. A. Lee, V. Vestman, A. Nautsch, M. Todisco, X. Wang, M. Sahidullah, J. Yamagishi, and D. A. Reynolds, “Tandem assessment of spoofing countermeasures and automatic speaker verification: Fundamentals,” *IEEE/ACM Transactions on Audio, Speech, and Language Processing*, vol. 28, pp. 2195–2210, 2020.